Self-Organized Bursts of Coherent Stimulated Raman Scattering and Hot Electron Transport in Speckled Laser Plasma Media

L. Yin, B. J. Albright, H. A. Rose, K. J. Bowers, B. Bergen, and R. K. Kirkwood

Phys. Rev. Lett. **108**, 245004 — Published 12 June 2012

DOI: 10.1103/PhysRevLett.108.245004

Self-organized bursts of coherent stimulated Raman scattering and hot electron transport in speckled laser plasma media

L. Yin[1], B. J. Albright[1], H. A. Rose[1], K. J. Bowers[1*], B. Bergen[1], R. K. Kirkwood[2]

[1] *Los Alamos National Laboratory, Los Alamos, New Mexico, 87545, USA*

[2] *Lawrence Livermore National Laboratory, Livermore, California 94550, USA.*

(Dated: March 13, 2012)

Abstract

Nonlinear electron trapping physics governs the onset and saturation of Stimulated Raman Scattering (SRS) in laser beams with many speckles. Hot electrons from intense speckles, produced during SRS daughter electron plasma wave bowing and filamentation, seed and enhance the growth of SRS in neighboring speckles by reducing Landau damping. Trapping-induced nonlinearity and speckle interaction through transport of hot electrons, backscatter, and sidescatter SRS waves enable the system of speckles to self-organize and exhibit coherent, sub-ps SRS bursts with more than 100% instantaneous reflectivity, consistent with an SRS transverse coherence width much larger than a speckle width.

PACS numbers: 52.38.Bv, 52.35.Mw, 52.35.Fp, 52.38.Dx

* Guest Scientist

Laser-plasma-interaction instabilities (LPI) feed off laser spatial coherence, so one of the first attempts at LPI control was through the introduction of finite coherence scales into the laser electromagnetic field, accomplished by a random phase plate [1] (RPP) optic element with a checkerboard pattern of random phase shifters in the far field. The resultant laser intensity pattern has coherence width (length) perpendicular (parallel) to the laser beam propagation $l_\perp \simeq F\lambda_0$ ($l_\parallel \simeq 10F^2\lambda_0$), where F is the optic F/# and λ_0, the laser wavelength. Regions of locally large laser intensity compared to the spatial average, speckles or intensity "hot spots", are quite elongated for $F = 8$, typical of the optic at the National Ignition Facility (NIF). Linear theory of stimulated Raman scatter [2] (SRS) from an isolated speckle qualitatively overestimates the threshold intensity for observable backscatter, as shown in experiment [3] and fully kinetic two- and three-dimensional (2D, 3D) simulations [4, 5]. Electron trapping in the SRS daughter electron plasma wave (EPW) significantly reduces Landau damping [6] and, hence, the SRS threshold in the trapping regime when $k\lambda_D \gtrsim 0.3$ (k is the EPW wave number and λ_D is the Debye length), as is typical of current laser-driven fusion experiments.

We report here evidence of large-scale, collective, self-organization arising in the nonlinear optics of plasmas, a high energy density physics "grand challenge" [7] area, from 2D kinetic simulations of SRS in the trapping regime in a many-$l_\perp$-wide homogeneous plasma slab containing more than 100 speckles. Our results manifest intense, sub-ps SRS bursts with *instantaneous* reflectivity $R_{\rm SRS} > 1$. The magnitude of the $R_{\rm SRS} > 1$ bursts, together with large system width, imply a transverse scattered light coherence width of order $\gg l_\perp$. We show in this Letter that this intermittent, global, transverse coherence is induced by speckle interaction through transport of SRS hot electrons, backscattered, and sidescattered light.

Our simulations employ the explicit, electromagnetic, particle-in-cell (PIC) code VPIC [8]. Absorbing boundary conditions are used for the fields and Maxwellian refluxing boundaries for the particles. The pump laser ($\lambda_0 = 351$ nm) propagates in the x direction. Temporally, it is a flat-top pulse with an average intensity $I_{\rm ave}$ launched from the left of the simulation domain; SRS is not explicitly seeded, but grows from thermal noise in the system. The simulation domain is in the (x, z) plane with size $L_x \times L_z$ μm. The plasma has a uniform density $n_e/n_{\rm cr} = 0.12$ and electron temperature of $T_e = 2.6$ keV ($k\lambda_D \simeq 0.3$; ions are immobile). The simulation cell size is $1.2 \times 1.7\lambda_D$, which resolves small-scale EPWs. The pump field E_y is specified at $x = 0$ in a manner that approximates a Gaussian random field,

which in vacuum creates a random distribution of F/8 speckles with characteristic width $l_\perp = 1.2F\lambda_0 = 3.4$ μm and length $l_\parallel = 2\pi F^2\lambda_0 = 141$ μm. For the speckle distributions used in the simulations, the intensity for the strongest speckle is typically 5 times the average intensity, but this can vary depending on the size of simulation domain and the random seed used; for large simulation domains, the strongest speckle's intensity with respect to the average is insensitive to the random seed. (Similar large-scale multi-speckle simulations have been used to successfully describe Raman amplification observed in experiments [9].)

For a simulation in domain 500×80 μm at $I_{\rm ave} = 2.9 \times 10^{14}$ W/cm^2, the pump field E_y is shown in the upper right panel in Fig. 1. In terms of the characteristic size of the speckles, the simulation region is 24 speckle widths and 3.5 speckle lengths (85 speckles total). These laser and plasma conditions are similar to those obtained in NIF ignition targets near the end of the laser pulse when SRS reflectivity is highest [10]. The reflectivity, shown in the upper left of Fig. 1, occurs in sub-ps bursts, as in single-speckle simulations [4, 5]. However, in a multi-speckled beam, the ensemble of uncorrelated laser speckles interact nonlocally and exhibit a transition to self-organized, collective behavior. A manifestation of this is the presence of intermittent, large bursts of SRS with $R_{\rm SRS} > 1$, indicated by the red arrows. We examine the quantity $\max\{-E_yB_z, 0\}$, proportional to the backscatter Poynting flux (in regions not dominated by forward-propagating laser light), and associate it with the SRS bursts to explain the interaction dynamics. In the simulation, strong speckles exhibit nonlinear SRS first, as indicated by the black arrow in the instantaneous reflectivity; the backscatter flux at $t = 1.5$ ps shown in the middle left panel results from these strong speckles at the location indicated by the while oval in the upper right frame. Strong speckles produce multiple SRS bursts during the simulation. Each burst produces EPWs that trap the electrons and the time-averaged electron velocity space distribution at the location of the strong speckles shows a strong trapping tail (shown in the inset in the middle left panel). While trapped electrons co-propagate with the SRS daughter EPW in the laser direction, they escape when the EPW amplitude decreases or through speckle side-loss, which occurs at a higher rate during SRS daughter EPW bowing and filamentation [4, 5] (side loss rate $\sim$ electron thermal velocity / EPW width).

We can estimate the hot electron transport time scale. The trapped electron resonant velocity is $\sim 4v_{\rm th}^e \simeq 0.28c$ (c is the speed of light) where $v_{\rm th}^e \simeq 0.07c$ is the electron thermal velocity. The trapped electron crossing time over a distance of 141 μm in the x direction,

the characteristic speckle length scale, is ~ 1.76 ps (the crossing time over the same distance for the back-scattered light is ~ 0.51 ps). The trapped electrons have a thermal velocity in the transverse direction, so over this interval they can travel ~ 35 μm in z. Thus, hot electrons produced from the first SRS burst shown in the middle left panel can travel deeper into the plasma by 141 μm in x in 1.76 ps and their spatial spread in z can span nearly the entire 80-μm z-domain. This forward and lateral inter-speckle hot electron transport is a critical part of the collective behavior of nonlinear SRS: hot electrons reduce Landau damping and the SRS onset threshold in neighboring speckles and in speckles deeper in the plasma (further away from the laser entrance boundary), where new SRS is initiated.

Prior single-speckle simulations [4, 11] show that EPW filamentation leads to SRS sidescatter at angles outside the incident laser cone [11] and that the sidescatter angle increases with EPW nonlinear frequency shift [11]. Similarly, in a multi-speckled beam, when a strong speckle exhibits nonlinear SRS, strong sidescatter occurs. As SRS light in a localized speckle propagates towards the laser entrance, it acts as an antenna seeding new SRS growth transversely in neighboring speckles through sidescatter. The time-averaged SRS spectral power as a function of transverse wavenumber $k_z\lambda_D$ measured at the laser entrance in the lower inset in Fig. 1 shows that SRS peaks at $k_z\lambda_D \sim \pm 0.01$. From the initial SRS matching conditions, $k_x\lambda_D = -0.1$. Thus, SRS spectral power peaks at angle $\theta \sim \pm 5.7^\circ$ with respect to $-\widehat{\boldsymbol{x}}$ outside the incident laser cone angle ($\pm 1/(2F) \sim \pm 3.6^\circ$). As a consequence of trapping induced EPW filamentation and sidescatter, SRS wavefronts from a localized speckle form the SRS "wake": within an intense speckle, trapping leads to a nonlinear frequency shift that down-shifts the EPW frequency, up-shifts the scattered light, and thus increases the phase speed of the scattered light above that outside the speckle. This causes scattered light to travel faster at the speckle center (in z) than at its edge, leading to wavefronts that bend (the amount of bending is consistent with the sidescatter angle), as shown by the inset in the middle right frame. Strong SRS in one speckle can thus couple to its neighbors, seeding strong SRS in these speckles, leading to SRS wakes (or sidescatter) propagating from these speckles to their neighbors, etc., creating a backward propagating SRS "avalanche" throughout the network of speckles with a transverse scattered light coherence width far greater than that of an individual speckle.

On the other hand, trapping-induced EPW spatial localization within a speckle in the transverse direction leads to rapid EPW dissipation [4, 5] and the resulting short time

scale multiplied by the scattered light group velocity sets the short length scale in the laser direction for the SRS to be much shorter than the speckle length; because the backscatter in neighboring speckles is seeded from the original speckle, the ensuing, collective burst of SRS in many speckles has a correspondingly short coherence length. This gives rise to a wide (in space), short-duration (sub-ps) burst of SRS reflectivity measured at the simulation boundary seen, e.g., around 4 ps when instantaneous reflectivity $R_{\rm SRS} > 1$.

Thus, the SRS dynamics of uncorrelated speckles are linked by the transport of SRS hot electrons (forward and transversely), collective backscatter, and sidescatter (backward and transversely). These effects, in turn, act back upon the original strong speckles. As a result, the strong speckles that produce the first SRS bursts continually emit strong bursts of SRS. Meanwhile, new SRS is also continuously initiated deeper in the plasma. The snapshot at $t = 9.4$ ps in the middle right panel shows new SRS deeper in the plasma (seen near $x \sim 320$ μm) as well as strong SRS from the strong speckles on the left. A later snapshot at $t = 9.9$ ps in the lower left panel displays two groups of unstable speckles localized in x but spread in z linked together by the backscattered and sidescattered light, while the lower right panel at $t = 10.6$ ps shows a time when all speckles near the left simulation boundary have became unstable and contribute to the largest SRS burst measured around $t = 10.7$ ps. These self-organized, collective, nonlinear SRS dynamics are shown in the simulation movie accompanying Fig. 1.

Because of trapping and speckle interaction, ensembles of speckles thus collectively lower the SRS onset threshold. (Note that the threshold for nonlinear SRS effects in a speckled laser field may be reduced compared to that of a coherent beam even without electron trapping through speckle intensity fluctuations and diffraction: the latter weakens SRS gain in any single speckle and couples one speckle's SRS to others' [12]). To quantitatively demonstrate this, SRS vs. average intensity scaling for collections of speckles with different transverse size are shown in Fig. 2 (for plasma and laser conditions the same as in Fig. 1). The black diamonds are from simulations at a domain size of 500×20 μm (3.5 speckle lengths and 6 speckle widths), whereas the triangles are from simulations of size 500×160 μm (48 speckle widths). Both systems show a sharp onset of SRS at a threshold laser intensity and saturation at higher intensity, as in isolated speckles [3–5]. Although the system length is the same in the two sets of simulations, the wider system allows more speckles to interact before scattered light escapes through the system's sides, which leads to a lower onset threshold

and more enhanced SRS at different laser intensity. The lower frames show instantaneous reflectivity for the larger simulation domain $I_{\rm ave} = 1.2$ and 2.9×10^{14} W/cm^2, respectively. More sub-ps bursts of SRS are observed as intensity increases and each burst saturates through trapping effects. Again, the SRS instantaneous reflectivity shows that large bursts with $R_{\rm SRS} > 1$ can occur over a short, sub-ps duration, made possible by speckles acting coherently. The average intensity for the lower frame in Fig. 2 is the same as in Fig. 1 and the instantaneous reflectivity from both shows qualitatively similar slow-varying time scales, namely, the first large burst with $R_{\rm SRS} > 1$ occurs before 4 ps and the large bursts with $R_{\rm SRS} > 1$ occurs among smaller bursts in groups separately by a slower time scale of ~ 4 ps. For the middle frame in Fig. 1, the average laser intensity is lower and trapping effects are weaker than in the high intensity system in the lower frame; thus, the first large burst with $R_{\rm SRS} > 1$ occurs later in time, after ~ 4 ps.

These dynamics are verified by scaling studies varying system dimension and laser intensity. For given L_z and $I_{\rm ave}$, results show that the coherence width increases with L_x. The instantaneous reflectivity from simulations for $L_z = 160$ μm at $I_{\rm ave} = 1.2 \times 10^{14}$ W/cm^2 are compared as L_x increases from 500 (black) to 1500 μm (red) in the middle frame in Fig. 1; the coherence width is found to increase by nearly a factor of 3, from ~ 70 μm to ≥ 160 μm. In larger L_x simulations, as time increases, new SRS initiates deeper in the plasma due to forward hot electron transport effects on intense enough speckles. As SRS event from these speckles propagates back to the laser entrance, it tends to spread due to SRS backscatter and sidescatter and therefore evolves to a larger collective burst with coherence width increasing as it propagates. However, this trend cannot continue indefinitely in the presence of multiple interacting SRS wakes (we observe that there can be several of these SRS events across the width of the plasma for sufficiently wide systems). For given L_x and L_z, the coherence width also increases with $I_{\rm ave}$ (as expected since sidescatter angle increases with speckle intensity); for the top frame in Fig. 2, the coherence width increases from ~ 70 μm to ~ 160 μm as $I_{\rm ave}$ changes from 1.2 to 5.6×10^{14} W/cm^2. On the other hand, coherence width (and time averaged reflectivity) is comparable, $\simeq 40 - 70$ μm, for $L_x = 500$ μm at $I_{\rm ave} = 1.2 \times 10^{14}$ W/cm^2 but with different $L_z = 40$, 80, 160, and 320 μm.

In summary, trapping-induced nonlinearity and speckle interaction through transport of SRS hot electrons, backscatter, and sidescatter light dramatically increases the transverse SRS coherence width to scales much larger than speckle width, while the self-organized large

SRS bursts occur in regions shorter than a speckle length due to transverse spatial localization of EPW within speckles. Together, this leads to coherent, sub-ps SRS bursts with $R_{\rm SRS} > 1$. The nonlinear SRS dynamics of uncorrelated speckles are linked by the forward and lateral transport of hot electrons and by the collective SRS light propagating backward and laterally. Ensembles of speckles thus collectively lower the SRS onset threshold relative to isolated speckle models [5]. Although the nonlinear trapping effects and SRS sidescatter are absent, preliminary paraxial three-wave model [13] results (with diffraction) exhibit similar SRS coherency behavior. Aside from their practical application to laser-energy coupling in ICF, these results are also important from the standpoint of basic physics: they represent a clear instance where an ensemble of uncorrelated optical elements in a nonlinear optical system exhibits a transition to self-organized, collective behavior. Existing diagnostic techniques [14], which may enable sub-ps resolution of backscattered and sidescattered SRS, would allow experimental validation of these results.

This work was performed under the auspices of the U.S. Dept. of Energy by the Los Alamos National Security, LLC Los Alamos National Laboratory and was supported by DOE NNSA Funding for ICF and by the LANL Directed Research and Development (LDRD) Program. VPIC simulations were run on ASC Roadrunner and Cielo. The authors acknowledge stimulating discussions with Drs. D. S. Montgomery and B. Afeyan.

[1] Y. Kato, *et al.*, Phys. Rev. Lett. **53**, 1057 (1984).

[2] M. V. Goldman and D. F. Du Bois, Phys. Fluids **8**, 1404 (1965).

[3] D. S. Montgomery, *et al.*, Phys. Plasmas **9**, 2311 (2002).

[4] L. Yin, *et al.*, Phys. Rev. Lett. **99**, 265004 (2007); L. Yin, *et al.*, Phys. Plasmas **15**, 013109 (2008).

[5] L. Yin, *et al.*, Phys. Plasmas **16**, 113101 (2009).

[6] Thomas O'Neil, Phys. Fluids **8**, 2255 (1965).

[7] Rosner, R. and D. Hammer, Report of the 2009 Workshop on Basic Research Needs for High Energy Density Laboratory Physics; Chairs: R. Rosner and D. Hammer, (http:science.energy.govfesnews-and-resourcesworkshop-reports)

[8] K. J. Bowers, *et al.*, Phys. Plasmas **15**, 055703 (2008); K. J. Bowers, *et al.*, Proceedings of

the ACM/IEEE conference on Supercomputing, Austin, 2008 (Piscataway, NJ, USA: IEEE Press) pp 1-11; K. J. Bowers, *et al.*, J. Phys.: Conf. Ser. **180**, 012055 (2009).

[9] R. K. Kirkwood, *et al.*, J. Plasma Phys. **77**, 521 (2010).

[10] R. K. Kirkwood, *et al.*, Phys. Plasmas **18**, 056311 (2011); S. H. Glenzer, *et al.*, Phys. Rev. Lett. **106**, 085004 (2011); D. E. Hinkel, *et al.*, Phys. Plasmas **18**, 056312 (2011).

[11] P. E. Masson-Laborde, *et al.*, Phys. Plasmas **17**, 092704 (2010).

[12] H. A. Rose and P. Mounaix, Phys. Plasmas **18**, 042109 (2011).

[13] T. Kolber, W. Rozmus and V. T. Tikhonchuk, Physics of Fluids B: Plasma Physics **5**, 138 (1993).

[14] R. Trebino, FROG: The measurement of Ultrashort Laser Pulses (Springer, 2002).

FIG. 1: (Color) Upper frames: Reflectivity (left), showing sub-ps bursts from a simulation in a domain 500×80 μm at $I_{\rm ave} = 2.9 \times 10^{14}$ W/cm^2 with the pump field E_y (right); the black arrow indicates the first SRS burst from strong speckles in the while oval; $R_{\rm SRS} > 1$ bursts are indicated by the red arrows. Middle and lower frames: Snap shots of quantity $\max\{-E_y B_z, 0\}$, proportional to the backscatter Poynting flux, showing spatial locations of SRS bursts. Middle left inset: time-averaged (over simulation duration 13.36 ps) electron velocity space distribution measured at the location of the strong speckles (spatially averaged over $\sim \lambda_{\rm EPW}$), showing a strong trapping tail. Middle right inset: The $E_y(x,z)$ field containing both laser and the scattered light wavefronts distinguished by their different wavelengths (as labeled). SRS backscatter light wave bowing occurring in multiple speckles with two strong speckles centered around $z = 14$ and 23 μm. Lower right inset: Time-averaged (over $\sim$ 13 ps) SRS spectral power as a function of transverse wavenumber $k_z\lambda_D$ measured at the laser entrance.

FIG. 2: (Color) Top: Time averaged SRS reflectivity vs. laser average intensity for collections of speckles in domains 500×20 μm [black diamonds; using 512 (65) particles per cell for the four lower intensity runs (at higher intensity)] and 500×160 μm [black triangles; using 512 (65) particles per cell for the two lower intensity runs (at higher intensity)] using density $n_e/n_{\rm cr} = 0.12$ and $T_e = 2.6$ keV ($k\lambda_D = 0.31$). Middle: Instantaneous reflectivity for 500×160 μm (black) and 1500×160 μm (red) simulations at $I_{\rm ave} = 1.2 \times 10^{14}$ W/cm^2. Lower: Instantaneous reflectivity for the 500×160 μm simulation at $I_{\rm ave} = 2.9 \times 10^{14}$ W/cm^2.

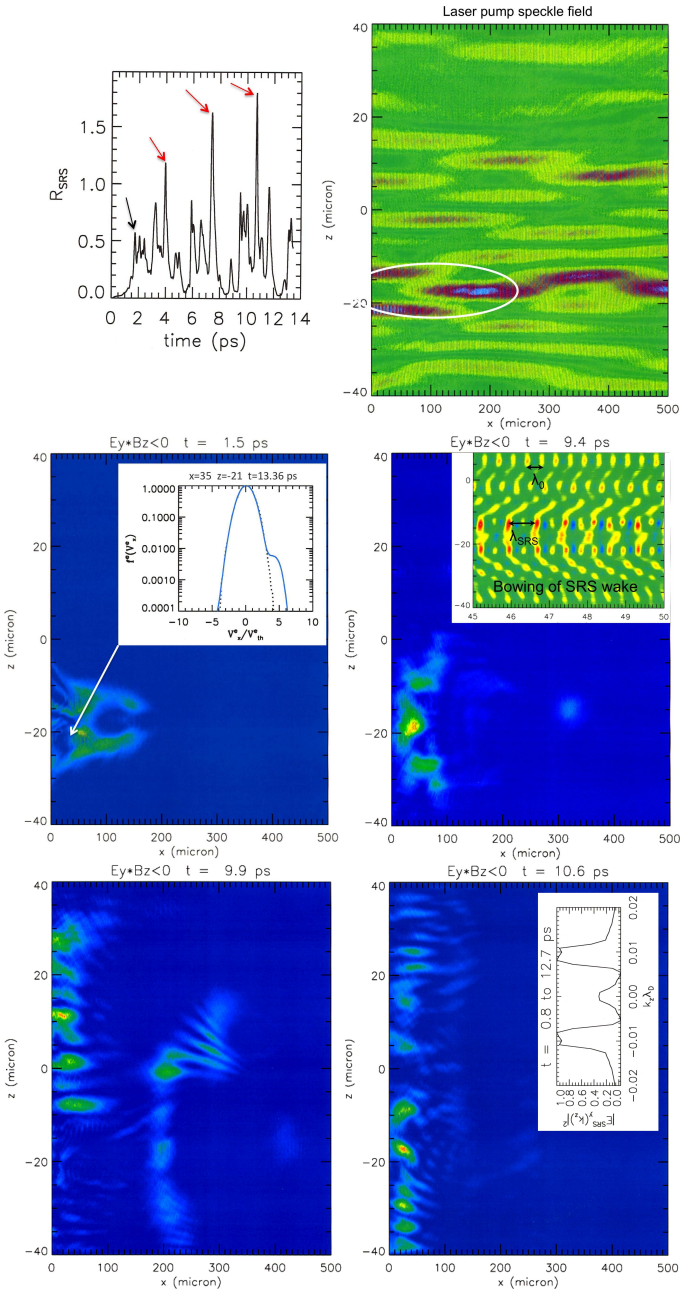

FIG. 1.

Figure 1 LM13033 13Mar2012

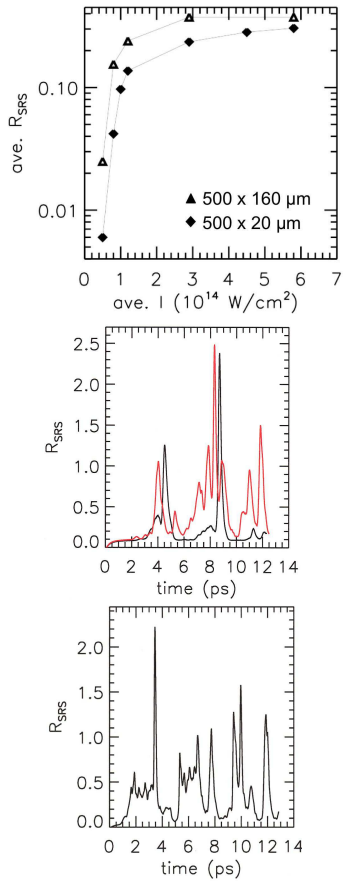

FIG. 2.

Figure 2 LM13033 13Mar2012